Ultrafast Microwave-Assisted Route to Surfactant-Free Ultrafine Pt Nanoparticles on Graphene: Synergistic Co-reduction Mechanism and High Catalytic Activity

ARTICLE *in* CHEMISTRY OF MATERIALS · JUNE 2011

Impact Factor: 8.35 · DOI: 10.1021/cm200329a

6 AUTHORS, INCLUDING:

Paromita Kundu
Forschungszentrum Jülich
29 PUBLICATIONS **520** CITATIONS
SEE PROFILE

Michael Rajamathi
St. Joseph's College of Bangalore
75 PUBLICATIONS **2,598** CITATIONS
SEE PROFILE

Giridhar Madras
Indian Institute of Science
553 PUBLICATIONS **9,737** CITATIONS
SEE PROFILE

CHEMISTRY OF MATERIALS

ARTICLE

pubs.acs.org/cm

Ultrafast Microwave-Assisted Route to Surfactant-Free Ultrafine Pt Nanoparticles on Graphene: Synergistic Co-reduction Mechanism and High Catalytic Activity

Paromita Kundu,[†] C. Nethravathi,[†] Parag A. Deshpande,[‡] M. Rajamathi,[§] Giridhar Madras,[‡] and N. Ravishankar*[,†]

[†]Materials Research Centre, and [‡]Department of Chemical Engineering, Indian Institute of Science, Bangalore 560012, India

[§]Department of Chemistry, St. Joseph's College, Bangalore, India

Supporting Information

ABSTRACT: We demonstrate an ultrafast method for the formation of graphene supported Pt catalysts by the co-reduction of graphene oxide and Pt salt using ethylene glycol under microwave irradiation conditions. Detailed analysis of the mechanism of formation of the hybrids indicates a synergistic co-reduction mechanism whereby the presence of the Pt ions leads to a faster reduction of GO and the presence of the defect sites on the reduced GO serves as anchor points for the heterogeneous nucleation of Pt. The resulting hybrid consists of ultrafine nanoparticles of Pt uniformly distributed on the reduced GO susbtrate. We have shown that the hybrid exhibits good catalytic activity for methanol oxidation and hydrogen conversion reactions. The mechanism is general and applicable for the synthesis of other multifunctional hybrids based on graphene.

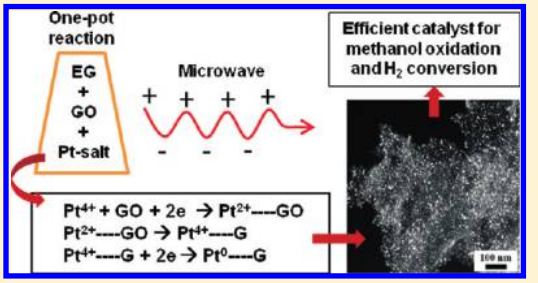

KEYWORDS: microwave reduction, graphene, supported catalyst, ultrafine Pt, methanol oxidation

INTRODUCTION

Graphene is one of the most fascinating materials today with a potential for a wide range of applications in nanoelectronics,[1−4] catalysis, capacitors,[5] and sensors.[6,7] Its excellent physical and chemical properties including mechanical strength and strain,[8] high thermal conductivity,[9] electron mobility,[10] and chemical inertness make it an ideal support material for noble metal nanocatalysts.[11] Carbon-based supports with Pd, Au, or Pt nanoparticles have already been demonstrated to exhibit high efficiencies for hydrogen storage,[12] CO oxidation, oxygen reduction reaction,[13] electrochemical sensing,[7] and in fuel cell applications.[7,8,14−19]

The direct methanol fuel cell (DMFC) produces electric power by the direct conversion of methanol and has attracted considerable attention as a clean power source.[20] However, the efficiency of DMFC is low because of the lower rate of methanol decomposition. Because of the high cost associated with the Pt electrocatalyst, it is necessary to develop new catalyst materials or improve the efficiency of existing catalysts and supports for methanol oxidation.[21] In addition, the elimination of hydrogen from the exhaust gases is important. Catalytic hydrogen combustion (CHC) is the process of H_2-O_2 recombination to yield water. While the oxidation of hydrogen by electrochemistry is well-known,[22,23] new nonelectrocatalysts are required to process large volumes of exhaust gas with complete oxidation of hydrogen. Hydrogen is well-known to dissociate over Pt; the support material also plays a crucial role in the catalytic activity of the material. Thus, there is a strong motivation to increase the utilization of catalysts via their dispersion as small particles on a support material. Other than high chemical stability and a large surface area, the support can also play a role in altering the electronic character and the geometry of the catalyst particles dispersed on the system.[24,25] Pt nanostructured catalysts on high area carbon[26,27] and crystallographically oriented manganese oxide nanorods[28] have been used for methanol oxidation and oxygen reduction reactions. In some cases, the support may participate in the reaction by utilizing surface hydroxyl groups and the lattice oxygen, as shown recently for Pt over ZrO_2 and TiO_2 supported catalysts for the catalytic hydrogen combustion reaction.[29]

Synthesizing hybrids of ultrafine nanoparticles on different supports remains a challenge in terms of controlling the particle size, distribution, and the thermal and/or electrochemical stability of catalyst under different operating conditions. Most current methods employ surfactants to control the size of the nanoparticles; however, for catalytic applications, it may be desirable to synthesize uncapped particles that exhibit similar or higher stability as compared to their capped counterparts.[30] Microwave heating methods have emerged as interesting alternatives for synthesizing a variety of materials/hybrids.[31] However, the mechanism of formation of the hybrids is not well understood. In this study, we

Received: December 12, 2010
Revised: March 23, 2011
Published: May 10, 2011

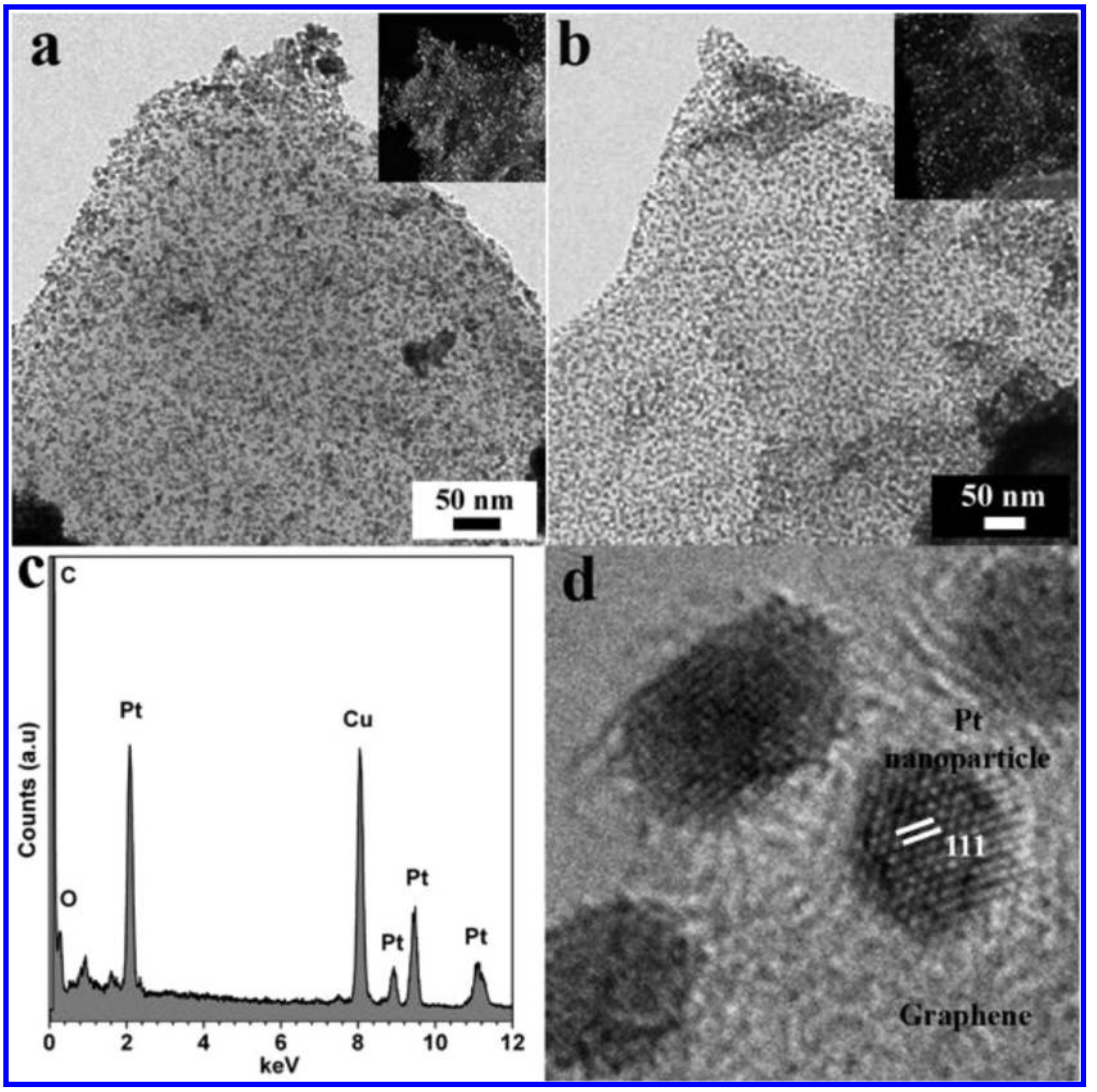

Figure 1. TEM bright-field image of (a) G−Pt(v1) and (b) G−Pt(v2) with corresponding dark-field images as insets, showing the particle size and uniform distribution on the sheets. The dark-field micrograph reveals the lesser density of particles in case of G−Pt(v2), that is, when a higher volume of EG was used. Part (c) shows the EDS analysis done on the hybrid G−Pt(v1) and gives an estimate of the density of the Pt nanoparticles on the RGO. (d) HR image of Pt nanoparticles on the RGO sheets.

describe an ultrafast, single-step microwave route to graphene−Pt nanohybrids in which ultrafine Pt nanoparticles (2−3 nm diameter) are distributed uniformly on a reduced graphene oxide (RGO) surface. The detailed investigation of the mechanism of the formation of the hybrids points to a synergistic co-reduction mechanism where the presence of Pt ions accelerates the reduction of graphite oxide to graphene under microwave irradiation conditions while the presence of the defect sites on the graphene surface promotes the heterogeneous nucleation of the Pt^{2+} intermediate and Pt^0 nanoparticles in a stepwise reduction process leading to ultrafine anchored nanoparticles of Pt on the RGO surface.[32,33] The hybrids exhibit excellent activity for methanol oxidation coupled with good long-term stability and also show enhanced catalytic activity for the hydrogen combustion reaction.

EXPERIMENTAL SECTION

Synthesis of Graphite Oxide (GO). GO used in the synthesis was prepared by the Hummers and Offeman method[34] from graphite powder (10−20 μm) supplied by Graphite India Limited, Bangalore, India. The details of the synthesis procedure followed are similar to those of our previous study.[18]

Synthesis of Graphene−Pt (G−Pt) Nanohybrid. For synthesizing the nanohybrid, G−Pt(v1), 5 mg of GO was dispersed in 20 mL of ethylene glycol (EG) by sonication for 30 min. The solution was allowed to cool to room temperature followed by the addition of 2 mg of chloroplatinic acid ($H_2PtCl_6 \cdot xH_2O$). Mild shaking dissolves the salt in EG, and the solution was subjected to microwave (MW) heating for four cycles of 50 s ON−10 s OFF in a domestic microwave oven (2.45 GHz) operated at 800 W. At the end of the heating, the solution was cooled to room temperature, and the product was isolated by several washes with distilled water to remove the excess EG and subsequent centrifugation at 2000 rpm for 5 min. The resulting product was washed with a minimum amount of acetone and dried in air. Samples for characterization were prepared by dispersing the product in distilled water. Similarly, G−Pt-(v2) was synthesized using 50 mL of EG, keeping the rest of the synthesis conditions identical. For making the G−Pt nanohybrids with lower loadings of Pt, only the starting amount of GO was varied in each case, keeping all other conditions fixed. Three samples with starting GO:

dx.doi.org/10.1021/cm200329a |*Chem. Mater.* 2011, 23, 2772–2780

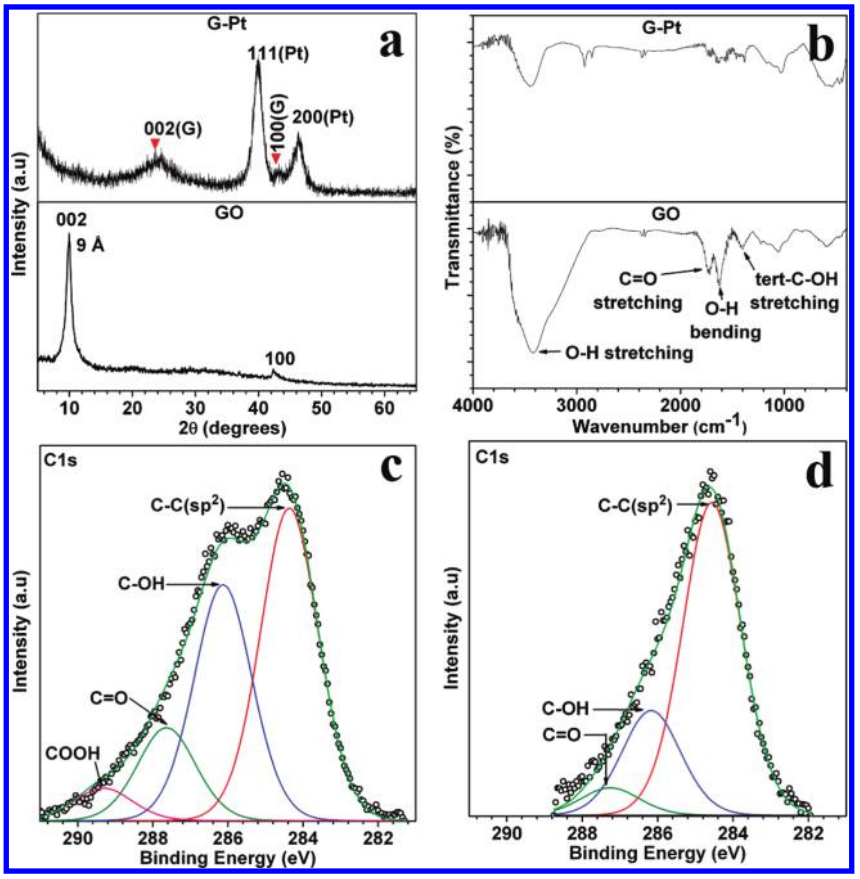

Figure 2. (a) XRD pattern from pristine GO (lower layer) and nanohybrid showing peaks due to Pt and graphene/graphite sheets (upper layer). (b) IR spectra of the GO (in lower layer) and the G−Pt (upper layer) showing the characteristic stretching frequencies for the functionalities on the graphene and the change in intensity on reduction of the GO. (c) C1s core level XPS of pristine GO before reaction. (d) C1s core level spectra from the final G−Pt nanohybrid showing considerable reduction of GO by decrease in the O-containing functional groups.

Pt salt ratios of 5:2 (GPt-1), 20:2 (GPt-2), and 40:2(GPt-3) were used for investigating the catalytic H_2 combustion reaction.

Control Experiments To Investigate the Mechanism of Formation of G−Pt Nanohybrid

(a) Reduction of GO to G in EG without Pt salt: The above procedure was followed without the addition of chloroplatinic acid.

(b) Synthesis of graphene−Pt (G−Pt) nanohybrid for shorter time: The procedure and quantity of GO and chloroplatinic acid remained the same as that for G−Pt(v1) except that only one cycle of microwave heating was performed.

(c) Reduction of GO in the presence of Pt nanoparticles: 2 mg of chloroplatinic acid ($H_2PtCl_6 \cdot xH_2O$) was dissolved in EG and subjected to MW heating for 50 s under the same conditions as above. About 1 mL aliquot of solution was collected for further characterization of the products. The rest of the solution was cooled to room temperature, and 5 mg of GO was added and sonicated. The mixture was again subjected to MW heating under the same conditions as above for four cycles of 50 s ON−10 s OFF.

(d) Synthesis of nanohybrids using graphitic carbon: In this case, the experimental conditions and methodology were the same as before except for using graphitic carbon (10−20 μm, supplied by Graphite India Limited, Bangalore, India) in place of GO at the start of the reaction.

(e) Synthesis of Pt nanoparticles: 2 mg chloroplatinic acid was dissolved in 20 mL of EG and subjected to microwave conditions as above for only 50 s. The product formed was isolated in the same manner as before.

Characterization. The powder X-ray diffraction (pXRD) patterns of the samples were recorded on a Philips X'pert Pro diffractometer (using Cu Kα radiation as source, secondary graphite monochromator, 2° 2θ per min). Infrared (IR) spectra were recorded on a Nicolet IR200 FTIR spectrometer (KBr pellets, 4 cm^{-1} resolution), XPS data were recorded on a ThermoScientific Multilab 2000 instrument, and the binding energies are with respect to graphitic C1s at 284.5 eV. FEI Tecnai T20 operating at 200 kV was primarily used for microscopy analysis and EDS analysis, and HRTEM was carried out in Tecnai F30 at 200 kV. Electrochemical measurements of G−Pt nanohybrid was carried out using cyclic voltammetry (CV) in PG26250, Techno Science Instrument in a conventional three-electrode system where a precleaned Pt foil was used as counter electrode and saturated calomel electrode (SCE) was used as the reference electrode.

Electrochemical Measurements. 10 mg of G−Pt nanohybrid was mixed with 20 mg of nafion followed by addition of isopropyl alcohol. The mixture was sonicated for 15 min to make a catalyst ink. The ink was then coated on a 0.5 cm × 0.5 cm graphite sheet. The electrodes were dried and weighed after drying. The loading of Pt on G−Pt was calculated from the TGA analysis for electrochemical analysis based on Pt content.

A three-electrode configuration conventional cell was used for all experiments. The electrolyte solutions were prepared using double-distilled water, and potential values are reported against SCE. The cell setup consisted of a glass chamber of about 70 mL capacity equipped with suitable ground-glass joints to introduce a working electrode, Pt foil auxiliary electrodes, and a saturated calomel electrode (SCE) as

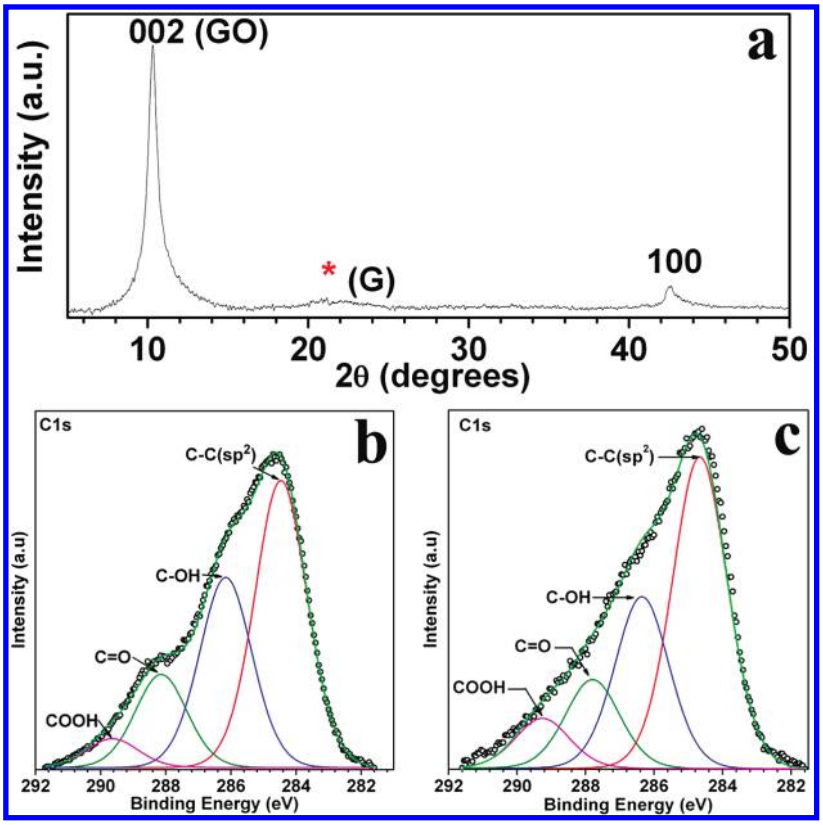

Figure 3. (a) XRD of GO after treating in EG in MW showing partial reduction/no reduction. Core level XPS spectra of C showing partial reduction of GO when subjected to reduction in EG in the absence of Pt salt (b) and in the presence of preformed Pt (c).

reference. The calculation of electrochemically active surface area (ECSA) of Pt nanoparticles was carried out using the hydrogen electro-sorption curve, recorded between −0.4 and +1.2 V in 1 M H_2SO_4 solution. The characteristic strong and weak peaks for adsorption/desorption of H_2 on the G−Pt nanohybrids were observed in the potential region of −0.25 to 0 V (vs SCE). The integrated area under the adsorption peak in the CV represents the total charge due to H^+ adsorption (Q_H) and was used to evaluate ECSA. The calculated ECSA is 90.92 m^2/g of Pt for the G−Pt nanohybrids (Supporting Information). To measure methanol electro-oxidation reaction activity, cyclic voltammetry was performed between 0 and +1.0 V in a solution containing 2 M CH_3OH and 1 M H_2SO_4 with a scan rate of 40 mV s^{-1}. Chronoamperometry was conducted at 0.7 V for 4 h.

Catalytic H_2 Combustion Reaction. The catalytic reactions were carried out in packed bed reactors. The reactors were made of glass tubes, and the catalysts were packed between the ceramic wool plugs. The length of the reactor was 35 cm while the catalyst bed length was 10 mm, and the catalyst bed was placed at the center of the reactor. The thermocouples were placed at the start and the center of the catalyst bed to ensure that the reaction was nearly isothermal. The temperature at the center of the catalyst bed was maintained using a standard PID controller, and all reactions were carried out isothermally.

The gases were monitored through a flow controller, and the hydrogen flow rate and oxygen flow rate were maintained at 5.5 and 2.75 mL/min, respectively. Thus, the inlet H_2 concentration of 2.75 mol % was maintained in all of the reactions to realize the actual fuel cell outlet conditions. N_2 was used as a diluent gas to ensure that the total flow rate was 200 mL/min in all cases. The gases exiting the reactor were analyzed using a gas chromatograph (Mayura Analyticals Pvt. Ltd., Bangalore, India) with nitrogen as the carrier gas and with a molecular sieve packed column and a thermal conductivity detector.

RESULTS AND DISCUSSION

A bright-field TEM image of ultrafine nanoparticles on the RGO substrate is shown in Figure 1a. Particle sizes of the order of 2−3 nm are seen in this image. The dark-field image (as inset) shows that the particles are well dispersed on the graphene surface, while the XEDS spectrum shown in Figure 1c confirms the presence of Pt. It has been reported that the exfoliated graphene functions better than graphite.[1,35,36] However, it has always been a challenge to obtain the desired single layer graphene in considerable yield for application. Recently, it has been achieved through solvation or intercalation of foreign moieties to separate graphene layers.[37] Ethylene glycol, being a polar solvent, increases the degree of exfoliation of the GO. To study its effect on the morphology of the nanohybrid, we investigated G−Pt nanohybrids, G−Pt(v1), and G−Pt(v2) synthesized using different volumes of EG. More EG is expected to improve the exfoliation of the sheets and offer higher surface area for the Pt nanoparticles to nucleate. Morphologically, we observed an increased interparticle spacing on the RGO sheets for G−Pt(v2) as compared to G−Pt(v1) as illustrated in Figure 1b. The inset to Figure 1b shows the dark-field image that shows the lower density of Pt on the sheets as compared to the G-Pt(v2). The analysis from different parts of the samples by TEM shows few aggregates of Pt nanoparticles on the sheets as well as outside for G−Pt(v1), whereas no aggregates could be seen for G−Pt(v2) on or outside the sheets (Supporting Information, Figure S1).

The high resolution image in Figure 1d illustrates that the particles are faceted (with interparticle spacing in the same order as that of the particle size). The analysis of several regions indicates

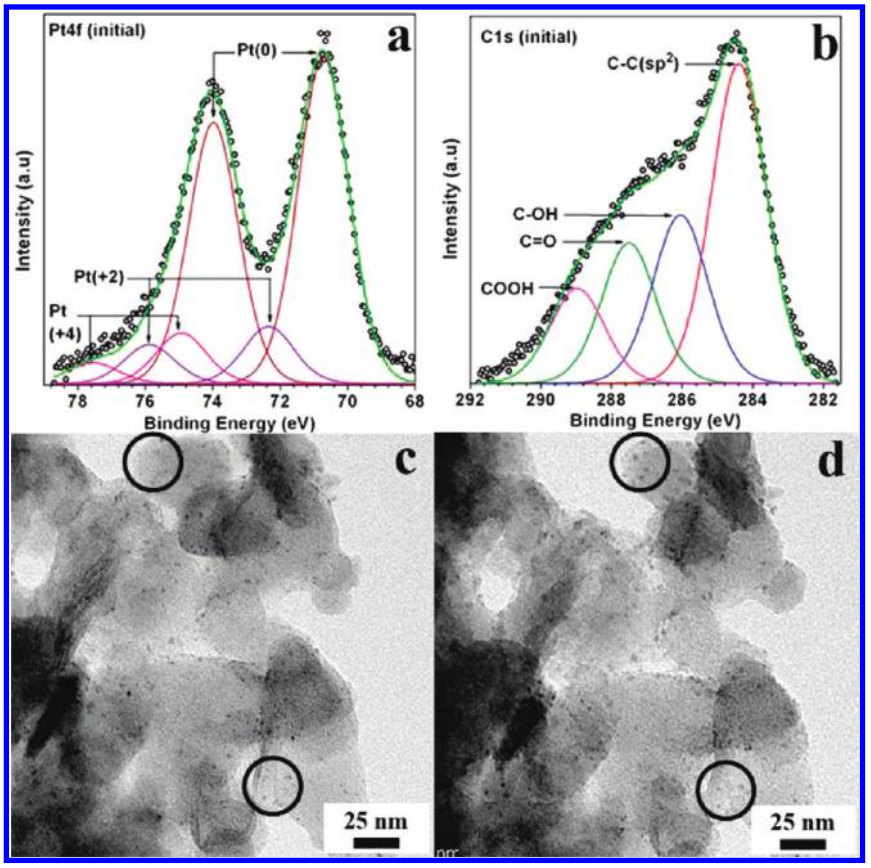

Figure 4. XPS of Pt (a) and C (b) in control experiment where G−Pt nanohybrid was at the initial stage of reaction after 50 s of microwave radiation. Bright-field TEM image of the same in (c) showing fewer Pt nanoparticles, indicating partial reduction of Pt salt. Part (d) shows the increase in Pt nanoparticle density due to reduction of the attached precursor under e-beam as illustrated in the circled region in the images.

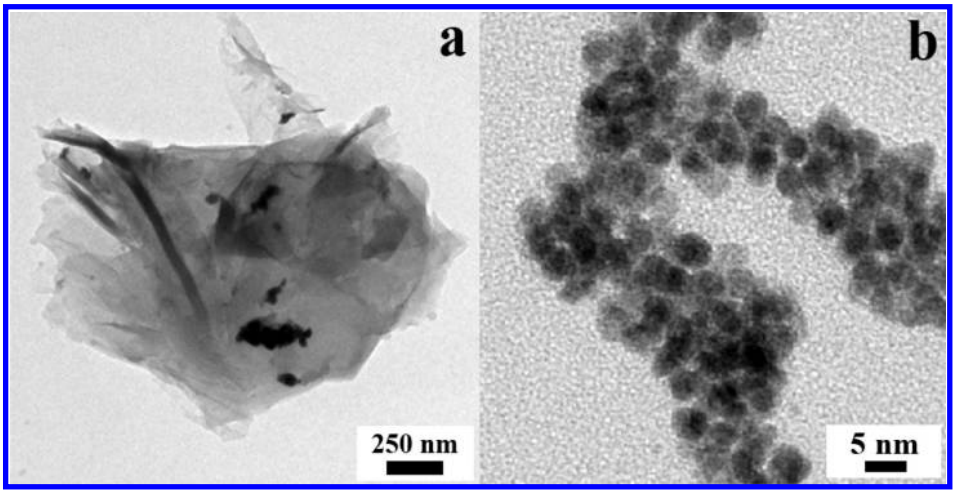

Figure 5. (a) TEM bright-field image of GO−Pt hybrid obtained by adding GO to reduced Pt and subjecting to microwave radiation (50 s on−10 s off cycle). It shows no attachment of Pt nanoparticles to the GO. (b) TEM bright-field image of Pt nanoparticles aggregate obtained by complete reduction of Pt salt in EG under MW radiation in 50 s.

that the Pt nanoparticles are always associated with the RGO sheets, indicating that these particles preferentially nucleate on this surface. We have observed that the density of particles on RGO could be tuned by changing the initial Pt salt concentration (Supporting Information, Figure S2). Figure 2 shows the powder XRD patterns of pristine GO before reaction and the final hybrid. While the pattern from GO in Figure 2a shows the prominent 002 peak corresponding to the layer spacing of stacked GO sheets before exfoliation, the characteristic peak corresponding to stacking of graphene sheets is seen in the reduced sample. A very broad (002) peak of the RGO is indicative of the high degree of exfoliation in this case. In addition, peaks corresponding to

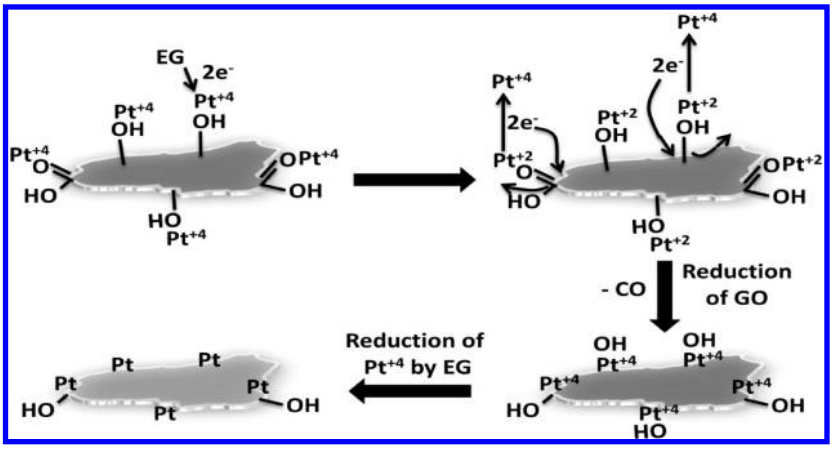

Figure 6. Schematic representation of synergistic co-reduction of GO and Pt-salt under microwave radiation.

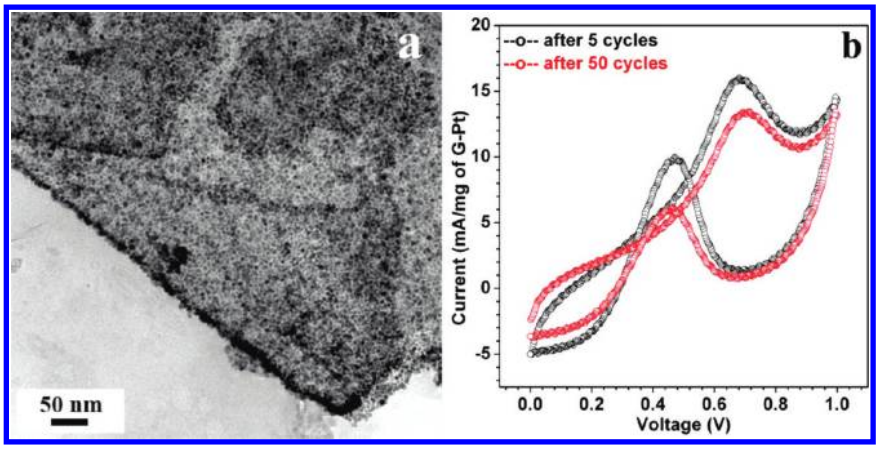

Figure 7. (a) TEM bright-field image of G−Pt hybrid obtained by using graphitic C and Pt-salt as starting material under the same conditions of microwave radiation as for GO. (b) CV of the graphitic−C−Pt nanohybrid yielding a forward current (I_f) of 15.99 mA/mg of the hybrid at the oxidation potential of 0.68 V. After 50 cycles, the potential shifts to 0.7 V yielding a current of 13.27 mA/mg of the hybrid. The current density thus calculated at the fifth cycle is 15.99 A/g of graphitic−C−Pt nanohybrid, and the tolerance (I_f/I_b) after 50 cycles was 1.2.

(111) and (200) planes of Pt are also observed. The IR spectrum from the hybrid (Figure 2b) in comparison to pristine GO indicates removal of functional groups from GO under the reaction conditions employed for synthesis. The C1s core-level X-ray photoelectron spectra (Figure 2c and d) also indicate key differences between the pristine GO and the sample subjected to microwave treatment. Figure 2d shows three distinct peaks corresponding to three different types of C, mainframe C (C═C sp^2) at 284.56 eV, C with the dangling OH groups or the epoxy linkage (C−OH/epoxy) at 286.17 eV, and the carbonyls (C═O) at 287.26 eV, while the pristine GO shows four different types of C (Figure 2c). A comparison of these two spectra shows the absence of the −COOH edge groups and a significant decrease in the intensity of the other functional groups. It is interesting to note that while reduction of GO under "dry" microwave conditions has been reported earlier,[5] obtaining a high degree of reduction in the solution phase has remained a challenge.[5,38]

Control experiments on GO in the absence of the Pt salt or microwave treatment in the presence of prereduced Pt nanoparticles only leads to partial reduction of GO. It is evident from the XRD pattern obtained from the GO subjected for reduction in microwave in the absence of Pt salt as given in Figure 3a. It was further confirmed from the core level XPS spectra of C obtained from GO in Figure 3b. In Figure 3c, the XPS analysis on the GO subjected to microwave-assisted reduction in the presence of prereduced metallic Pt also indicates partial reduction of GO, implying that only the Pt ions in the solution phase contribute to the reduction of GO. XPS analysis of samples irradiated for a shorter time indicates the presence of Pt^{4+} and Pt^{2+} states in addition to partially reduced GO (Figure 4a and b). TEM analysis of this sample shows the formation of Pt nanoparticles under the electron beam (Figure 4c and d), indicating that Pt ions are adsorbed on the sheets during the initial stages of the reaction. Thus, we can conclude that the presence of Pt ions in the solution phase aids in the reduction of GO. Moreover, Pt does not anchor to GO sheets when added separately as in the case of GO reduced in the presence of Pt nanoparticles as shown in Figure 5a. This implies that heterogeneous nucleation of the precursor phase (Pt^{2+}) and its subsequent site specific reduction to Pt^0 is a crucial step for the fine dispersion of the metal catalyst on RGO. Microwave irradiation of the Pt salt in the solution phase (in the absence of GO) leads to complete reduction in a short time and the formation of aggregates of Pt nanoparticles as evident from Figure 5b. XPS analysis (Supporting Information, Figure S3) of the product indicates that it is predominantly Pt^0

dx.doi.org/10.1021/cm200329a |*Chem. Mater.* 2011, 23, 2772–2780

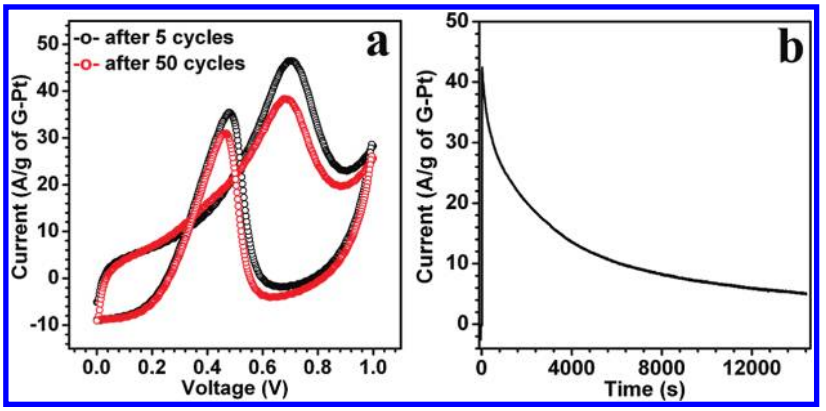

Figure 8. (a) Cyclic voltammogram obtained using the G−Pt(v1) hybrid as catalyst for methanol oxidation reaction (in solution containing 1 M H_2SO_4 and 2 M CH_3OH at a scan rate of 40 mV s^{-1}) and (b) the chronoamperometric study on the catalyst done for 4 h at 0.7 V for methanol oxidation reaction.

Table 1. Electrochemical Studies on the G−Pt Hybrids

sample	oxidation potential (V)	I_f/I_b	current density of G−Pt (A/g)
G−Pt(v1)	0.70	1.31	46.43
	0.68	1.24	38.26
G−Pt(v2)	0.64	1.46	16.53

with a small amount of +2 oxidation state corresponding to surface oxidation, as reported earlier.[17,18] In contrast, both Pt^{2+} and Pt^{4+} are present when the microwave irradiation is done in the presence of GO (Figure 4a). Thus, it is clear that the kinetics of Pt reduction is slower in the presence of GO. We propose that the Pt^{2+} plays a key role in the reduction of GO, and thereby gets oxidized to Pt^{4+}, as described by the equations below. This mechanism explains the slower kinetics of Pt reduction as well as the XPS results.

$$Pt^{4+} + GO + 2e \rightarrow Pt^{2+}\text{----}GO$$

$$Pt^{2+}\text{----}GO \rightarrow Pt^{4+}\text{----}G$$

$$Pt^{4+}\text{----}G + 2e \rightarrow Pt^{0}\text{----}G$$

A schematic illustration of the mechanism of formation is given in Figure 6. Sonication of GO in ethylene glycol leads to exfoliation of the sheets and the dissolution of the Pt salt to form Pt^{4+} ions in the solution. MW radiation polarizes the electron cloud and agitates the dipoles associated with the functional groups, creating active hot spots on the GO surface,[39] thereby leading to site-specific reduction of the precursor Pt^{4+} to Pt^{2+} by EG. We propose that the nucleated Pt^{2+} ions reduce GO, thereby getting oxidized to Pt^{4+}. This hypothesis also rationalizes the slow kinetics for reduction of Pt salt. The removal of the functional groups from the basal plane leads to the formation of defect sites[32] that serve as nucleation centers for the subsequent formation of Pt nanoparticles by EG reduction. Thus, a synergistic co-reduction mechanism whereby the Pt ions contribute to the reduction of GO and the defect sites on G contribute to the heterogeneous nucleation of Pt metal leads to the formation of a G−Pt composite with uniformly dispersed ultrafine nanoparticles on the surface. Although the functional groups on GO play an important role in anchoring and site-specific nucleation of the Pt nanoparticles, it is not a necessary condition for attachment of the Pt nanoparticles to the basal plane of G. This is indicated by control experiments performed with graphitic carbon as the support. We have seen that Pt nanoparticles nucleate on the sheets under similar condition with a good coverage over the sheets as illustrated in Figure 7a. Figure 7b shows the electrochemical behavior of the graphitic C−Pt sample where we observe a current density of 15.99 A/g of the hybrid with CO tolerance of 1.2. However, the particles in this case show aggregation in several regions and are also susceptible to coarsening by migration due to the lack of anchoring sites on the surface.[40−42]

For the G−Pt(v1) nanohybrid, the electrochemical surface area (ECSA) that relates to the accessible electrochemically active sites as estimated using the hydrogen adsorption/desorption peaks was found to be around 91 m^2/g of the hybrid (Supporting Information, Figure S4). The electrocatalytic activity of the nanohybrid G−Pt toward methanol oxidation was studied using cyclic voltammetry (Figure 8a). Methanol oxidation potential, current, and the tolerance (I_f/I_b) are shown in Table 1. The electrochemical behavior of the nanohybrid G−Pt is significantly improved as compared to reported literature values,[19,43−45] making it a potentially competitive electrocatalyst for fuel cell applications. The long-term oxidation of methanol using nanohybrid G−Pt was conducted at 0.7 V, and the variation of current with time was recorded for chronoamperometric study as given in Figure 8b. A steady-state oxidation current of 5 A/g (G/Pt) at the end of 4 h of experiment suggests a durable catalytic activity of the nanohybrid G−Pt for electrooxidation of methanol. The bright-field TEM image of the sample subjected to the steady-state experiments for 4 h shows no significant change in morphology (Supporting Information, Figure S5). It is interesting to note that the G−Pt(v1) nanohybrid is a better catalyst than graphitic C−Pt hybrid in terms of current density and CO tolerance, although morphologically both look similar. The ECSA, electrochemical performance, and durability of the nanohybrid G−Pt as a catalyst are significantly superior as compared to the recently reported Pt-based nanomaterials.[11,44] This could be attributed to the uniform spatial distribution, size control without surfactant, and attachment of the Pt nanoparticles on the defect sites of the high surface area graphene sheets. The presence of residual functional groups on the reduced GO could also contribute to the catalytic activity as

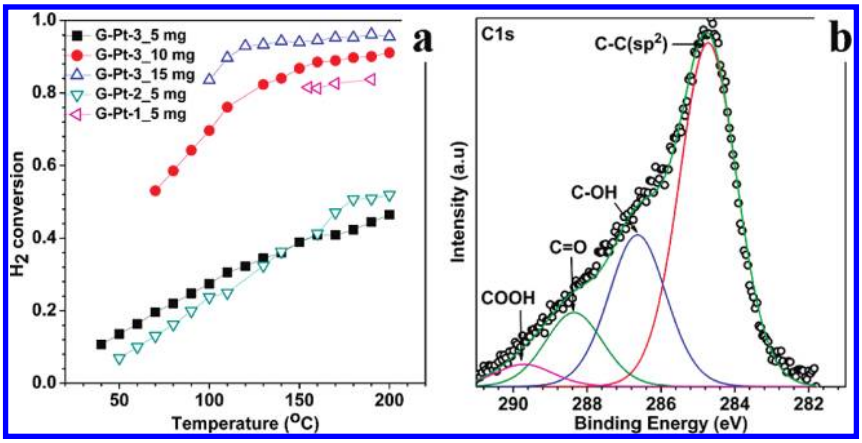

Figure 9. (a) Catalytic H_2 conversion (CHC) using the G−Pt nanohybrids and (b) the C1s core level XPS analysis where different functional moieties on the hybrid after CHC are indicated.

reported earlier.[46] The electrocatalytic behavior of the G−Pt(v2) looked more promising in terms of tolerance, but the current density was lower than that of G−Pt(v1) as given in Table 1 (Supporting Information, Figure S6). This could be due to the lower density of Pt particles per sheet in case of G−Pt(v2), which results in higher degree of exfoliation of the GO during synthesis. The higher CO tolerance in this case is thus an outcome of higher density of unreduced functional groups on RGO adjacent to Pt, which can oxidize the CO to CO_2, and is due to lower probability of coarsening locally during the electrochemical cycles.[41,42]

The variation of H_2 conversion with temperature is shown in Figure 9a. The initial experiments were carried out with 5 mg of GPt-*x* nanohybrids (*x* = 1, 2, 3). The concentration of hydrogen was held constant at 2.75 mol % (5.5 mL/min in 200 mL/min total gas flow) corresponding to operating fuel cell conditions. Three different O_2 concentrations were used: 1.375 mol % corresponding to stoichiometry (H_2:O_2 = 1:1), 2.75 mol % corresponding to twice the stoichiometry, and 21 mol % of oxygen corresponding to air. In the latter two cases, 100% conversion was obtained within 100 °C. With the stoichiometric amount of O_2 in the feed, at 200 °C around 50% conversion was obtained with 5 mg of GPt-2 and GPt-3, while around 85% conversion was obtained with 5 mg of GPt-1. Increasing the catalyst beyond 10 mg of GPt-1 resulted in complete conversion but resulted in very high temperature rise during the reaction, and isothermal conditions thus could not be maintained. Therefore, the amount of catalyst was varied only in case of GPt-3. At 140 °C, around 30% conversion was obtained with 5 mg of GPt-3, while around 85% and 95% conversions were obtained with 10 and 15 mg of GPt-3, respectively. These conversions at 140 °C are much higher than that reported in the literature.[29]

A reaction mechanism for CHC involves four main steps: (a) adsorption of H_2 over the noble metal catalyst, (b) reduction of the support, (c) splitting of O_2 from the stream and formation of H_2O, and (d) reoxidation of the support.[29] However, in this case, the support being RGO, it is more prone to get oxidized rather than getting reduced. So the primary mechanism involved here can be attributed to the adsorption of the H_2 on the Pt and the adsorption of O_2 on the adjacent C-framework of RGO. This is followed by combination of H_2 and O_2 to produce water. Because this reaction is exothermic, this results in the oxidation of the RGO support as well. This is evident from the C1s XPS as given in Figure 9b, which shows the presence of functional groups that were reduced when the hybrid was formed. Further, in the G−Pt hybrid, Pt was observed to exist in two mixed oxidation states, 0 and +2. However, Pt^{2+} is not in a completely ionic state, but its higher binding energy in XPS is due to its strong interaction with the support, as reported in previous studies.[42,47] After the CHC reaction, the relative intensity ratio of Pt(0):Pt(+2) increased due to the reducing nature of H_2. Therefore, we can conclude that the G−Pt hybrid with lower loading is a promising catalyst for CHC.

CONCLUSION

Our method opens up an ultrafast method to the synthesis of catalytically active graphene-based noble metal nanohybrid. It circumvents the issues related to exfoliation and reduction of the graphene support, on one hand, and size-controlled, uniform dispersion of the noble metal catalyst, Pt in this study, over the support, on the other hand. A mechanistic overview of the hybrid formation via microwave route has been investigated in detail here. The method is general and can be potentially applied to the synthesis of similar supported noble metal catalysts. The hybrid is a potential DMFC catalyst and also shows high CHC activity.

ASSOCIATED CONTENT

Supporting Information. Experimental details and additional figures. This material is available free of charge via the Internet at http://pubs.acs.org.

AUTHOR INFORMATION

Corresponding Author
*E-mail: nravi@mrc.iisc.ernet.in.

ACKNOWLEDGMENT

N.R. thanks DST, NSTI for financial support. The electron microscopes are a part of the Advanced Facility for Microscopy and Microanalysis at IISc.

REFERENCES

(1) Geim, A. K.; Novoselov, K. S. *Nat. Mater.* **2007**, *6*, 183–191.

(2) Li, X.; Wang, X.; Zhang, L.; Lee, S.; Dai, H. *Science* **2008**, *319*, 1229–1232.
(3) Pang, S.; Tsao, H. N.; Feng, X.; Müllen, K. *Adv. Mater.* **2009**, *21*, 3488–3491.
(4) Novoselov, K. S.; Jiang, D.; Schedin, F.; Booth, T. J.; Khotkevich, V. V.; Morozov, S. V.; Geim, A. K. *Proc. Natl. Acad. Sci. U.S.A.* **2005**, *102*, 10451–10453.
(5) Zhu, Y.; Murali, S.; Stoller, M. D.; Velamakanni, A.; Piner, R. D.; Ruoff, R. S. *Carbon* **2010**, *48*, 2118–2122.
(6) Fowler, J. D.; Allen, M. J.; Tung, V. C.; Yang, Y.; Kaner, R. B.; Weiller, B. H. *ACS Nano* **2009**, *3*, 301–306.
(7) Guo, S.; Wen, D.; Zhai, Y.; Dong, S.; Wang, E. *ACS Nano* **2010**, *4*, 3959–3968.
(8) Zhou, M.; Zhang, A.; Dai, Z.; Feng, Y. P.; Zhang, C. *J. Phys. Chem. C* **2010**, *114*, 16541–16546.
(9) William, J. E.; Lin, H.; Pawel, K. *Appl. Phys. Lett.* **2010**, *96*, 203112.
(10) Ghosh, S.; Calizo, I.; Teweldebrhan, D.; Pokatilov, E. P.; Nika, D. L.; Balandin, A. A.; Bao, W.; Miao, F.; Lau, C. N. *Appl. Phys. Lett.* **2008**, *92*, 151911−151911–151913.
(11) Seger, B.; Kamat, P. V. *J. Phys. Chem. C* **2009**, *113*, 7990–7995.
(12) Ströbel, R.; Garche, J.; Moseley, P. T.; Jörissen, L.; Wolf, G. *J. Power Sources* **2006**, *159*, 781–801.
(13) Li, F.; Yang, H.; Shan, C.; Zhang, Q.; Han, D.; Ivaska, A.; Niu, L. *J. Mater. Chem.* **2009**, *19*, 4022–4025.
(14) Yawen, T.; Lingling, Z.; Yanen, W.; Yiming, Z.; Ying, G. A. O.; Changpeng, L. I. U.; Wei, X.; Tianhong, L. U. *Preparation of a Carbon Supported Pt Catalyst Using an Improved Organic Sol Method and Its Electrocatalytic Activity for Methanol Oxidation*; Elsevier: Amsterdam, 2006.
(15) Wang, S.; Jiang, S. P.; White, T. J.; Guo, J.; Wang, X. *J. Phys. Chem. C* **2009**, *113*, 18935–18945.
(16) Sanles-Sobrido, M.; Correa-Duarte, M. A.; Carregal-Romero, S.; Rodriguez-Gonzalez, B.; Alvarez-Puebla, R. A.; Herves, P.; Liz-Marzan, L. M. *Chem. Mater.* **2009**, *21*, 1531–1535.
(17) Halder, A.; Sharma, S.; Hegde, M. S.; Ravishankar, N. *J. Phys. Chem. C* **2009**, *113*, 1466–1473.
(18) Nethravathi, C.; Anumol, E. A.; Rajamathi, M.; Ravishankar, N. *Nanoscale* **2011**, *3*, 569–571.
(19) Guo, S.; Dong, S.; Wang, E. *ACS Nano* **2010**, *4*, 547–555.
(20) Wasmus, S.; Küver, A. *J. Electroanal. Chem.* **1999**, *461*, 14–31.
(21) Liu, H.; Song, C.; Zhang, L.; Zhang, J.; Wang, H.; Wilkinson, D. P. *J. Power Sources* **2006**, *155*, 95–110.
(22) Elezovic, N. R.; Babic, B. M.; Vracar, L. M.; Radmilovic, V. R.; Krstajic, N. V. *Phys. Chem. Chem. Phys.* **2009**, *11*, 5192–5197.
(23) Uchida, H.; Izumi, K.; Aoki, K.; Watanabe, M. *Phys. Chem. Chem. Phys.* **2009**, *11*, 1771–1779.
(24) Park, I.-S.; Park, K.-W.; Choi, J.-H.; Park, C. R.; Sung, Y.-E. *Carbon* **2007**, *45*, 28–33.
(25) Gan, L.; Lv, R.; Du, H.; Li, B.; Kang, F. *Carbon* **2009**, *47*, 1833–1840.
(26) Park, S.; Xie, Y.; Weaver, M. J. *Langmuir* **2002**, *18*, 5792–5798.
(27) Jiang, J.; Kucernak, A. *J. Electroanal. Chem.* **2005**, *576*, 223–236.
(28) El-Deab, M. S.; Ohsaka, T. *Angew. Chem., Int. Ed.* **2006**, *45*, 5963–5966.
(29) Deshpande, P. A.; Madras, G. *Phys. Chem. Chem. Phys.* **2011**, *13*, 708–718.
(30) Chen, X.; Wu, G.; Chen, J.; Chen, X.; Xie, Z.; Wang, X. *J. Am. Chem. Soc.* **2011**, *133*, 3693–3695.
(31) Chen, W. X.; Lee, J. Y.; Liu, Z. *Chem. Commun.* **2002**, 2588–2589.
(32) Bagri, A.; Mattevi, C.; Acik, M.; Chabal, Y. J.; Chhowalla, M.; Shenoy, V. B. *Nat. Chem.* **2010**, *2*, 581–587.
(33) Kundu, P.; Halder, A.; Viswanath, B.; Kundu, D.; Ramanath, G.; Ravishankar, N. *J. Am. Chem. Soc.* **2010**, *132*, 20–21.
(34) Hummers, W. S.; Offeman, R. E. *J. Am. Chem. Soc.* **1958**, *80*, 1339–1339.
(35) An, X.; Simmons, T.; Shah, R.; Wolfe, C.; Lewis, K. M.; Washington, M.; Nayak, S. K.; Talapatra, S.; Kar, S. *Nano Lett.* **2010**, *10*, 4295–4301.
(36) Blake, P.; Brimicombe, P. D.; Nair, R. R.; Booth, T. J.; Jiang, D.; Schedin, F.; Ponomarenko, L. A.; Morozov, S. V.; Gleeson, H. F.; Hill, E. W.; Geim, A. K.; Novoselov, K. S. *Nano Lett.* **2008**, *8*, 1704–1708.
(37) Si, Y.; Samulski, E. T. *Chem. Mater.* **2008**, *20*, 6792–6797.
(38) Salas, E. C.; Sun, Z.; Luttge, A.; Tour, J. M. *ACS Nano* **2010**, *4*, 4852–4856.
(39) Bilecka, I.; Niederberger, M. *Nanoscale* **2009**, *2*, 1358–1374.
(40) Chan, K. T.; Neaton, J. B.; Cohen, M. L. *Phys. Rev. B* **2008**, *77*, 235430.
(41) Ishii, A. *J. Phys.: Conf. Ser.* **2008**, *100*, 052087.
(42) Yu, X.; Ye, S. *J. Power Sources* **2007**, *172*, 145–154.
(43) Xu, C.; Wang, X.; Zhu, J. *J. Phys. Chem. C* **2008**, *112*, 19841–19845.
(44) Gupta, G.; Slanac, D. A.; Kumar, P.; Wiggins-Camacho, J. D.; Kim, J.; Ryoo, R.; Stevenson, K. J.; Johnston, K. P. *J. Phys. Chem. C* **2010**, *114*, 10796–10805.
(45) Li, Y.; Gao, W.; Ci, L.; Wang, C.; Ajayan, P. M. *Carbon* **2010**, *48*, 1124–1130.
(46) Sharma, S.; Ganguly, A.; Papakonstantinou, P.; Miao, X.; Li, M.; Hutchison, J. L.; Delichatsios, M.; Ukleja, S. *J. Phys. Chem. C* **2010**, *114*, 19459–19466.
(47) Coloma, F.; Sepúlveda-Escribano, A.; Fierro, J. L. G.; Rodríguez-Reinoso, F. *Appl. Catal., A* **1996**, *148*, 63–80.